

# Degree of Permanent Densification in Oxide Glasses upon Extreme Compression up to 24 GPa at Room Temperature

Sung Keun Lee,\* Kwan Young Mun, Yong-Hyun Kim, Juho Lhee, Takuo Okuchi, and Jung-Fu Lin

Cite This: *J. Phys. Chem. Lett.* 2020, 11, 2917–2924

Read Online

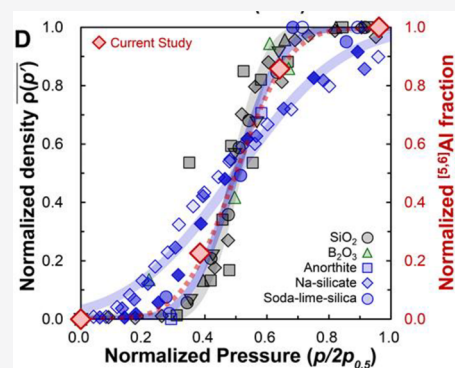
ACCESS |

Metrics & More

Article Recommendations

Supporting Information

**ABSTRACT:** During the decompression of plastically deformed glasses at room temperature, some aspects of irreversible densification may be preserved. This densification has been primarily attributed to topological changes in glass networks. The changes in short-range structures like cation coordination numbers are often assumed to be relaxed upon decompression. Here the NMR results for aluminosilicate glass upon permanent densification up to 24 GPa reveal noticeable changes in the Al coordination number under pressure conditions as low as  $\sim 6$  GPa. A drastic increase in the highly coordinated Al fraction is evident over only a relatively narrow pressure range of up to  $\sim 12$  GPa, above which the coordination change becomes negligible up to 24 GPa. In contrast, Si coordination environments do not change, highlighting preferential coordination transformation during deformation. The observed trend in the coordination environment shows a remarkable similarity to the pressure-induced changes in the residual glass density, yielding a predictive relationship between the irreversible densification and the detailed structures under extreme compression. The results open a way to access the nature of plastic deformation in complex glasses at room temperature.



The densification of noncrystalline materials can be achieved via the compression of liquids at high temperature and subsequent quenching at high pressure. In such a case, the structures of the quenched glasses represent those of supercooled liquids at high pressure and at the glass-transition temperature ( $T_g$ ), where the melt structures are frozen.<sup>1</sup> Alternatively, densified glasses can also be formed by compressing glasses at room temperature without melting (i.e., cold compression). After the decompression of cold-compressed glasses, most of their high-pressure structures revert back to the ambient-pressure structures. Nevertheless, some aspects of irreversible densification that occur upon cold compression may be preserved after the release of the pressure, manifesting as the remaining signatures of the high-pressure characteristics (i.e., permanent densification at room temperature). The nature of this densification has been primarily inferred from the diverse changes observed in the thermodynamic,<sup>2</sup> mechanical,<sup>3</sup> and elastic properties of permanently densified simple amorphous oxides, including  $\text{SiO}_2$  glass.<sup>4,5</sup> Densification in more complex oxide glasses accounts for their plastic deformation under pressure,<sup>6,7</sup> which is often accompanied by increased hardness.<sup>8–10</sup>

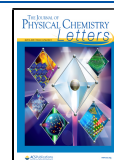
Whereas the atomistic origins of such irreversible densification are difficult to identify, the extent of deformation and permanent densification in glasses has often been attributed to topological changes in the glass networks, such as changes in the bond angle and length and in the ring size distribution,<sup>11–17</sup> and to structural rearrangements on an intermediate-range scale beyond the second coordination

environments (Supporting Information S1).<sup>18–23</sup> Therefore, the detailed short-range structures, such as the coordination environments around framework cations (e.g., Si and Al), have not often been considered to contribute to permanent densification at room temperature.<sup>24–26</sup> Indeed, highly coordinated cations, such as  $^{[4]}\text{B}$  and  $^{[5]}\text{Si}$ , transition back into the coordination states prevalent at 1 atm ( $^{[3]}\text{B}$  and  $^{[4]}\text{Si}$ ) during decompression from 23 GPa for  $\text{B}_2\text{O}_3$  glass<sup>27,28</sup> and from 40 GPa for  $\text{SiO}_2$  glass.<sup>29–31</sup> Molecular dynamics simulations have shown that the coordination transformations that occur at high pressure may not be quenched upon decompression,<sup>32</sup> resulting in reversion back to the coordination environments that are stable at 1 atm.<sup>33</sup> In contrast, other theoretical studies have shown that a portion of the  $^{[5,6]}\text{Si}$  that is present at high pressure may be preserved upon decompression if the peak pressure is sufficiently high.<sup>34</sup> The irreversible densification of glasses is promoted under the high-temperature conditions relevant to shock-induced dynamic compression,<sup>35–38</sup> whereas postannealing often removes any high-pressure signatures. Structural studies at relatively low pressures ( $\sim 2$  GPa) and near  $T_g$  have revealed coordination

Received: March 4, 2020

Accepted: March 28, 2020

Published: March 28, 2020



changes.<sup>9,39,40</sup> Whereas these changes are relatively minor, the glasses compressed in this regime often show greater permanent densification, with data confirming the effect of composition. For example, a significant change in the cation coordination numbers in densified Li-aluminoborate glasses only up to 2 GPa was observed, accounting for the improved crack resistance and the enhanced residual density.<sup>41</sup> Therefore, the nature of the structural transformation in prototypical aluminosilicate glasses that is expected to occur under much higher pressure conditions (>20 GPa) at room temperature needs to be confirmed because the ability of glasses to deform is inextricably related to the changes in coordination numbers that occur under extreme compression.<sup>42–44</sup> The potential changes in coordination environments under permanent densification at room temperature also provide improved insights into crack initiation and its propagation during the indentation<sup>41</sup> and ductile deformation of noncrystalline materials at low temperature.<sup>6,45</sup>

Mg-bearing aluminosilicate glasses are technically important optical and refractive glasses (ref 46 and references therein). Because Mg, Si, Al, and O are among the most abundant elements in the Earth's mantle, Mg<sub>3</sub>Al<sub>2</sub>Si<sub>3</sub>O<sub>12</sub> (pyrope) glass serves as a reference for the behavior of iron-free mantle melts in the Earth's interior and is a simplified model basaltic glass. In particular, multicomponent basaltic glasses in subducting cold oceanic crust may undergo an irreversible structural transition during subduction and a subsequent rapid ascent at relatively low temperature, potentially below its  $T_g$ . Pyrope glass, which consists of two major framework cations (Si and Al), may allow us to reveal the element-specific densification paths of an amorphous oxide undergoing permanent densification. Whereas a preferential coordination transformation in amorphous oxides has been proposed,<sup>47</sup> a systematic relationship between the transition pressure and the types of cations in permanently densified glasses under extreme compression remains to be established. High-resolution solid-state nuclear magnetic resonance (NMR) provides information on the cation coordination numbers and the atomic configurations around O atoms bonded to Si and Al (i.e., bridging oxygen (BO)) and network modifiers (e.g., Mg<sup>2+</sup>) (i.e., nonbridging oxygen (NBO)) at high pressure (Supporting Information S2).<sup>47–52</sup>

The structural transitions in irreversibly densified pyrope glass are manifested in multinuclear (<sup>17</sup>O, <sup>27</sup>Al, and <sup>29</sup>Si) NMR spectra. Figure 1 (left) shows the <sup>27</sup>Al MAS NMR spectra of

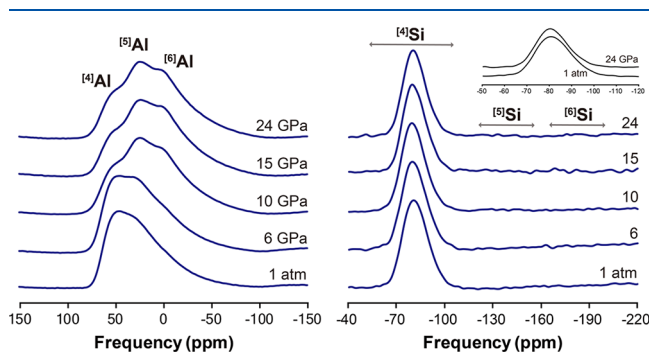


**Figure 1.** (Left) <sup>27</sup>Al MAS NMR spectra for irreversibly densified Mg<sub>3</sub>Al<sub>2</sub>Si<sub>3</sub>O<sub>12</sub> (pyrope) glasses with varying peak pressures as labeled. (Right) <sup>29</sup>Si MAS NMR spectra for decompressed pyrope glasses after cold compression up to 24 GPa, as labeled. Enlarged NMR spectra at 1 atm and 24 GPa are shown as an inset.

Mg<sub>3</sub>Al<sub>2</sub>Si<sub>3</sub>O<sub>12</sub> glass at 1 atm and decompressed glass with varying peak pressures up to 24 GPa. Under ambient pressure conditions, the dominant peak is observed at ~60 ppm, corresponding to four-coordinated Al ([<sup>4</sup>]Al). Small features corresponding to [<sup>5</sup>]Al and [<sup>6</sup>]Al (at ~30 and 0 ppm, respectively) are also observed. As the decompression pressure (i.e., the peak pressure at which the decompression starts) increases, the [<sup>5,6</sup>]Al peak intensity also increases above ~6 GPa, providing unambiguous evidence of the changes in short-range structures in oxide glasses during permanent densification. By contrast, the <sup>29</sup>Si NMR spectra of the glass show a peak that is only due to [<sup>4</sup>]Si, regardless of the decompression pressure, up to 24 GPa (Figure 1, right). The presence of [<sup>5,6</sup>]Si species is negligible with a detection limit of ~1%. This indicates that the permanent densification in aluminosilicate glasses at room temperature primarily involves Al. The current results confirm that some portion of [<sup>5,6</sup>]Al is quenchable upon decompression to 1 atm, making it a useful structural indicator of the permanent densification in oxide glasses. To further quantify the changes in the Al coordination transition, 2D <sup>27</sup>Al triple-quantum (3Q) MAS NMR spectra were collected, revealing well-resolved peaks corresponding to [<sup>4,5,6</sup>]Al (Figure 2). A noticeable fraction of [<sup>5,6</sup>]Al peaks can be observed in the spectra of the glass decompressed from pressures above 5 GPa. The [<sup>5,6</sup>]Al peak intensity drastically increases up to ~15 GPa. Above 15 GPa, no additional changes in the Al coordination environment are observed. Figure 2 (right) also presents the isotropic projection of the <sup>27</sup>Al 3QMAS NMR spectra. Here the 2D NMR spectrum was further sheared to yield robust estimates of the [<sup>4,5,6</sup>]Al fractions (Supporting Information S3). The projected spectra confirm that a drastic increase in the fraction of [<sup>5,6</sup>]Al species occurs only from ~5 up to ~15 GPa.

The nature of permanent densification is also manifested in the pressure-induced changes in the oxygen environments. Figure 3 (bottom) shows the <sup>17</sup>O 3QMAS NMR spectra for decompressed Mg<sub>3</sub>Al<sub>2</sub>Si<sub>3</sub>O<sub>12</sub> glass that has undergone cold compression up to 24 GPa. The spectrum at 1 atm shows oxygen peaks stemming from distinct NBO and BO species, corresponding to Mg–O–[<sup>4</sup>]Si (~–32 ppm in the isotropic dimension), [<sup>4</sup>]Si–O–[<sup>4</sup>]Al (~–36 ppm), and [<sup>4</sup>]Si–O–[<sup>4</sup>]Si (~–48 ppm). (See ref 46 and references therein.) A non-negligible fraction of [<sup>4</sup>]Al–O–[<sup>4</sup>]Al species is also evident (~–21 ppm in the isotropic dimension). The peak intensity at ~–43 ppm increases as the decompression pressure increases (Figure 3 (top), isotropic projection of the spectra). This peak corresponds to BO linking [<sup>4</sup>]Si and [<sup>5,6</sup>]Al (i.e., [<sup>4</sup>]Si–O–[<sup>5,6</sup>]Al).<sup>53,54</sup> In contrast, the intensity of Mg–O–[<sup>4</sup>]Si decreases with increasing pressure. Therefore, the formation of the [<sup>5,6</sup>]Al in the permanently densified aluminosilicate glass (Figures 1 and 2) results from the annihilation of Mg–NBO by forming [<sup>4</sup>]Si–O–[<sup>5,6</sup>]Al.<sup>46</sup>

We note that during the static compression of aluminosilicate glasses and melts, the [<sup>5,6</sup>]Al fraction gradually increases over a wide range of pressures (>~30 GPa).<sup>53–55</sup> By contrast, the coordination transformation during permanent densification occurs within only a narrow pressure span of ~7 GPa (Figures 1 and 2). Figure 4A shows that the [<sup>5,6</sup>]Al fraction increases with increasing decompression pressure from ~6% (at 1 atm) to ~13% (at 6 GPa). Whereas the change in the [<sup>n</sup>]Al fraction may be minor below 5 GPa, the [<sup>5,6</sup>]Al fraction drastically increases with increasing decompression pressure starting at ~6 GPa up to ~33% (at 10 GPa). Above 15 GPa,

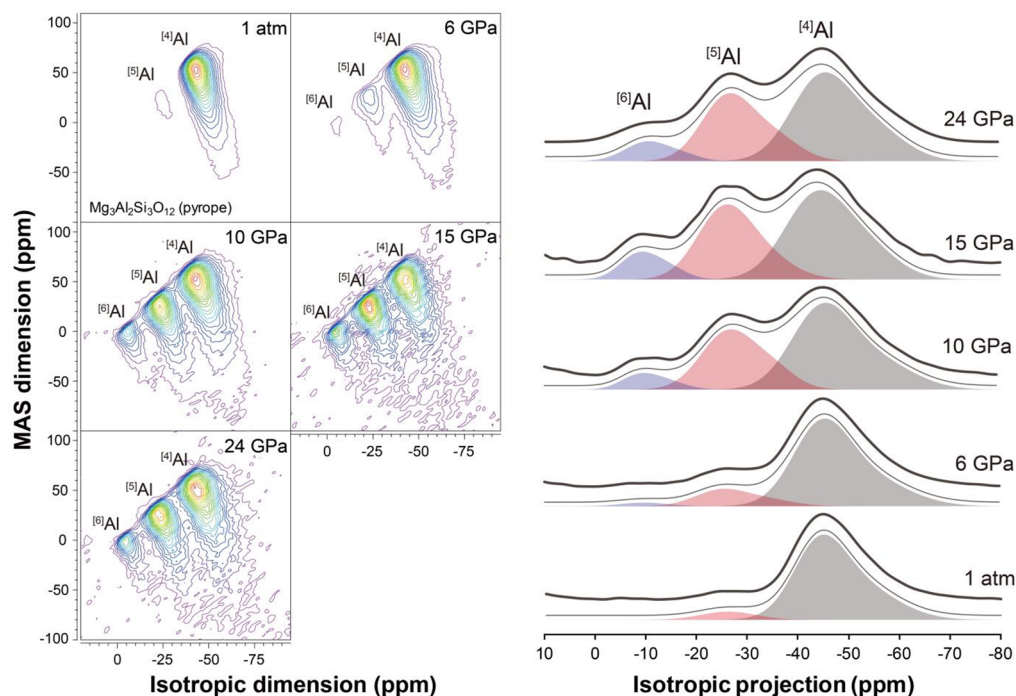


**Figure 2.** (Left)  $^{27}\text{Al}$  3QMAS NMR spectra for decompressed  $\text{Mg}_3\text{Al}_2\text{Si}_3\text{O}_{12}$  glasses after cold compression up to 24 GPa, as labeled. Contour lines are drawn from 3–98% of relative intensity with a 5% increment. (Right) Total isotropic projection of  $^{27}\text{Al}$  3QMAS NMR spectra for decompressed  $\text{Mg}_3\text{Al}_2\text{Si}_3\text{O}_{12}$  glasses after cold compression up to 24 GPa. Results of fitting with multiple Gaussian functions (thin black lines) to the isotropic projection of  $^{27}\text{Al}$  3QMAS NMR spectra for  $\text{Mg}_3\text{Al}_2\text{Si}_3\text{O}_{12}$  glasses are shown. The thick lines represent the experimental spectra. The spectra were fitted using multiple Gaussian functions representing  $^{[n]}\text{Al}$  species.

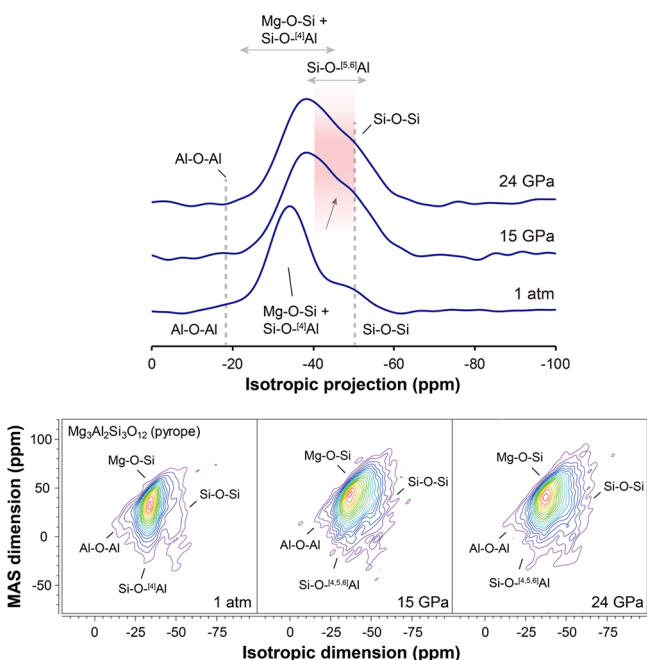


**Figure 3.** Total isotropic projection (top) and full 2D (bottom)  $^{17}\text{O}$  3QMAS NMR spectra for decompressed  $\text{Mg}_3\text{Al}_2\text{Si}_3\text{O}_{12}$  glasses after cold compression up to 24 GPa. Contour lines are drawn from 3 to 98% relative intensity with a 5% increment.

the Al coordination apparently reaches a plateau (with  $^{[5,6]}\text{Al}$  fraction of  $\sim 38\%$ ) for pressures at least up to 24 GPa.

The changes in the Al coordination environment in the irreversibly densified glass allow us to describe the nature of permanent densification. Figure 4B presents the variation of

the normalized  $^{[4,5,6]}\text{Al}$  fraction,  $\overline{X^{[n]}\text{Al}(p)}$ , with varying decompression pressures. Here the difference between the  $^{[4,5,6]}\text{Al}$  fraction at a given pressure  $[X^{[n]}\text{Al}(p)]$  and that at 24 GPa  $[X^{[n]}\text{Al}_{24\text{GPa}}]$  is normalized with respect to that between the  $^{[4,5,6]}\text{Al}$  fractions at 1 atm  $[X^{[n]}\text{Al}_{1\text{atm}}]$  and 24 GPa (i.e.,  $[X^{[n]}\text{Al}(p) - X^{[n]}\text{Al}_{24\text{GPa}}]/[X^{[n]}\text{Al}_{1\text{atm}} - X^{[n]}\text{Al}_{24\text{GPa}}]$ ). At least three distinct pressure ranges of structural transitions involving Al coordination transformations are identified. In the initial stage of densification (Region I), an increase in the decompression pressure may not result in a major increase in the  $^{[5,6]}\text{Al}$  fraction. The potential changes in the coordination environments during compression, if any, are also expected to be reversible (i.e., elastic), permitting reversion to the 1 atm configurations. Region II is a transition zone characterized by a dramatic coordination transformation in an intermediate pressure range (from  $\sim 5$  to  $\sim 12$  GPa, as marked by shaded areas). The transition zone for pyrope glass may start at the threshold pressure ( $\sim 5$  GPa), where the short-range structures begin to change as part of permanent densification (i.e., undergo an elastic–plastic transition in the coordination number). At the high-pressure boundary of the transition zone ( $\sim 12$  GPa), the coordination change becomes negligible. Region III spans from  $\sim 12$  to  $\sim 24$  GPa; in this region, the change in the  $^{[5,6]}\text{Al}$  fraction is again negligible. We find that the three-step paths in  $X^{[n]}\text{Al}(p)$  can be well described with the following model based on the complementary error function (erfc) (Supporting Information S3)

$$\overline{X^{[5,6]}\text{Al}(p)} = 1 - \frac{1}{2} * \text{erfc}\left(\frac{p - p_{0.5}}{\alpha}\right) \quad (1)$$

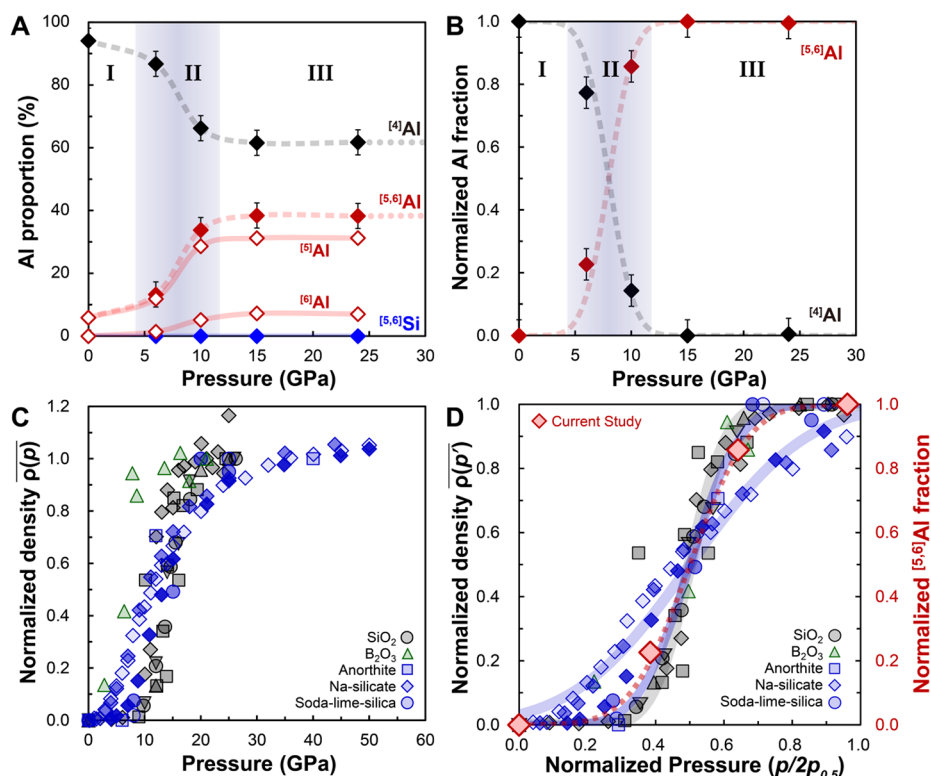


**Figure 4.** (A) Variation of the proportions of four- (black rhomboids), five-, and six-coordinated Al (red rhomboids) in cold-compressed pyrope glasses with varying peak pressures from 1 atm to 24 GPa. The blue shaded area indicates the pressure range of drastic coordination environments for Al atoms from 4 to 5 and 6. (B) Variation of normalized  $^{[4,5,6]}\text{Al}$  fraction,  $\overline{X^{[n]}\text{Al}(p)}$ , with varying peak pressures (i.e.,  $[X^{[n]}\text{Al}(p) - X^{[n]}\text{Al}_{24\text{GPa}}]/[X^{[n]}\text{Al}_{1\text{atm}} - X^{[n]}\text{Al}_{24\text{GPa}}]$ ). Three distinct pressure ranges of structural transitions involving Al coordination transformation are labeled I, II, and III, respectively. (See the main text.) (C) Variation of normalized residual density,  $\overline{\rho(p)}$  ( $= (\rho(p) - \rho_{1\text{atm}})/(\rho_{\text{max}} - \rho_{1\text{atm}})$ ) with respect to varying pressures in oxide glasses. Displayed glasses include  $\text{SiO}_2$  glass (gray symbols: rhombohedron,<sup>61</sup> square,<sup>2</sup> triangle,<sup>62</sup> circle,<sup>63</sup> inverted triangle<sup>12</sup>),  $\text{B}_2\text{O}_3$  glass (green triangle<sup>60</sup>), anorthite glass (blue square<sup>73</sup>), alkali silicate glasses (dark blue, rhombohedron ( $\text{Na}_2\text{O}/\text{SiO}_2$  5:95), blue rhombohedron ( $\text{Na}_2\text{O}/\text{SiO}_2$  15:85), and pale blue rhombohedron ( $\text{Na}_2\text{O}/\text{SiO}_2$  30:70)<sup>10</sup>), and soda-lime-silica glasses (blue circle,<sup>8</sup> blue pale circle<sup>62</sup>). (D) Renormalized fractions of  $^{[5,6]}\text{Al}$  and residual  $\overline{X^{[5,6]}\text{Al}(p')}$  and  $\overline{\rho(p')}$  with normalized pressure  $p'$  ( $= p/2p_{0.5}$ ). (See the main text.) Red rhomboids indicate normalized  $^{[5,6]}\text{Al}$  proportion to normalized pressure. Legends for other symbols are the same as panel C. Trend lines were modeled using eqs 4 and 5.

$$\overline{X^{[4]}\text{Al}(p)} = \frac{1}{2} * \text{erfc}\left(\frac{p - p_{0.5}}{\alpha}\right) \quad (2)$$

where  $p_{0.5}$  is the transition pressure at which  $\overline{X^{[n]}\text{Al}(p)}$  reaches 50% of its maximum value and  $\alpha$  is a constant related to the flexibility of the degree of amorphous network pressurization.<sup>50</sup> A larger  $\alpha$  results in a structural transition over a broader pressure range. We find that this model with a  $p_{0.5}$  of  $\sim 7.8$  GPa and an  $\alpha$  of  $\sim 3$  provides a good description of the observed Al coordination transformation in pyrope glass. This trend indicates that the structural transitions that occur due to the permanent densification of glasses may originate from the distribution of the transition pressures for coordination transformation due to the intrinsic structural disorder that is prevalent in amorphous oxides.<sup>56,57</sup>

The onset of permanent densification in an oxide glass can be identified from an increase in the residual glass density.<sup>58</sup> The change in the residual density upon decompression is nonlinear and is most notable within a relatively narrow pressure range (Figure 4C). For example, no residual densification is observed for  $\text{SiO}_2$  glass at decompression pressures up to  $\sim 5$  GPa; the residual density then abruptly increases at pressures up to 15 GPa, and no further changes in densification have been observed up to  $\sim 30$  GPa.<sup>2</sup> Figure 4C

displays such changes in the normalized residual densities of diverse oxide glasses with the decompression pressure.<sup>2,12,59–63</sup> Here we have normalized the residual densities of the compressed glasses  $[\overline{\rho(p)} = (\rho(p) - \rho_{1\text{atm}})/(\rho_{\text{max}} - \rho_{1\text{atm}})]$  such that they vary from 0 to 1 (Supporting Information S4). Whereas the  $\overline{\rho(p)}$  values show complex composition dependence, the variation is similar to the trend observed in Figure 4B. Therefore, a similar model using the error function can be used to describe the pressure-induced change in the residual density

$$\overline{\rho(p)} = 1 - \frac{1}{2} * \text{erfc}\left(\frac{p - p_{0.5}}{\alpha'}\right) \quad (3)$$

where  $\alpha'$  is a constant similar to  $\alpha$  in eq 1 and describes the degree of change in the residual density upon decompression. The remarkable similarity between  $\alpha$  and  $\alpha'$ , and thus the similarity in the overall pressure dependence, indicates that the observed Al coordination transformation mainly reflects an increase in the residual density. The estimated  $p_{0.5}$  and  $\alpha'$  values of the oxide glasses are summarized in Table S1. By introducing the normalized pressure  $p'$  ( $= p/2p_{0.5}$ ) (here  $p_{0.5}$  is the pressure at which the residual density is  $0.5 * (\rho_{\text{max}} - \rho_{1\text{atm}})$ ), we can determine the normalized residual density as a function of  $p'$ ,  $\overline{\rho(p')}$ , allowing us to compare the pressure-

induced changes in residual density that are observed for diverse oxide glasses

$$\overline{\rho(p')} = 1 - \frac{1}{2} \text{erfc} \left( \frac{p' - 1/2}{\alpha'} \right) \quad (4)$$

Similarly,  $\overline{X^{[5,6]}\text{Al}(p')}$  can be described as follows

$$\overline{X^{[5,6]}\text{Al}(p')} = 1 - \frac{1}{2} \text{erfc} \left( \frac{p' - 1/2}{\alpha} \right) \quad (5)$$

Figure 4D shows the variation of  $\overline{\rho(p')}$  for diverse oxide glasses, confirming that the trend of the permanent densification in oxide glasses can be well described by eq 4.

The mole fractions of  $^{[n]}\text{Al}(\overline{X^{[n]}\text{Al}(p')})$  in the current study are also shown. The trends in  $\overline{\rho(p')}$  and  $\overline{X^{[5,6]}\text{Al}(p')}$  are similar, indicating that the three-step paths (Figure 4B), and thus the changes in both the structures and the properties described in eqs 1–5, are also prevalent in diverse irreversibly densified oxide glasses. Whereas the effect of the composition on the nature of the permanent densification and residual density of these glasses remains to be investigated, the observed trend shown in Figure 4B–D is expected to hold, in general, for oxide glasses, accounting for bonding changes in numerous glass-forming oxide materials during their plastic deformation under extreme compression. Previous studies have explored relationship structural transitions in the permanently densified glasses and their bulk density under low-pressure conditions up to 2 GPa and under elevated temperature conditions near  $T_g$ , revealing that the changes in the coordination environment may partially contribute to the changes in the bulk density.<sup>6,41,45,64</sup> In contrast, the current study revealed the relations between residual densification and structural compaction at much higher pressure conditions above 20 GPa and room temperature. The detailed changes in the fraction of structural units and the residual density in the permanently densified glasses under extreme compression can both be described with the simple analytical model (eqs 3 and 5). This conceptual advance allows us to quantify the degree of permanent densification in glasses under extreme compression above 20 GPa.

We note that the change in glass density upon compression is reported to correlate well with structural compaction, in particular, oxygen packing density.<sup>64,65</sup> Recent high-pressure studies of glasses under static compression confirmed that the average O–O distance reduction accounts for the increase in the bulk density of the glasses.<sup>44,66</sup> The evolution of the glass density of compressed glasses has also been modeled using the differences in partial molar volumes of each distinct coordination polyhedron (e.g.,  $\text{AlO}_4$  and  $\text{AlO}_5$ ).<sup>67</sup>

The current results allow us to trace the structural changes in two distinct framework cations (i.e., Si and Al) during compression and subsequent decompression, demonstrating a distinct difference in the responses of Si (>24 GPa) and Al (~5 GPa) under varying decompression pressures (Figure 4A). Whereas the Si coordination environment may change upon compression up to 24 GPa,<sup>34,68</sup> the lack of any observed change in the Si coordination environment indicates that  $^{[5,6]}\text{Si}$  may transform back into  $^{[4]}\text{Si}$  during decompression and that the Si coordination transformation into  $^{[5,6]}\text{Si}$  is partially suppressed during compression. This preferential coordination transformation of Al over Si and the distinct threshold pressure for each cation arise from the difference in their electronic

structures. Specifically, the transition pressure for the significantly more contracted electron distribution in Si, which has an atomic radius of 1.1 Å, is higher than that in Al with an atomic radius of 1.26 Å at ambient pressure.<sup>47</sup> The atomic radii of the framework cations in oxide glasses determine the nature of permanent densification. Whereas experimental confirmations of element-specific threshold pressures for other complex oxide glasses are left for future work, complex glasses may exhibit similar trends in terms of irreversible structural transitions.

The experimental verification of the coordination transformations occurring in amorphous oxides undergoing permanent densification has remained challenging in the study of the physical chemistry of glasses. In this study, we report multinuclear NMR results for aluminosilicate glass undergoing permanent densification. The unambiguous evidence of the presence of high-energy, short-range structures and their transformation with a narrow pressure window allow us to microscopically constrain the multiple irreversible deformation paths of diverse amorphous materials.<sup>6,45</sup> Permanently densified Mg-bearing aluminosilicate glass may have implications for the deformation of noncrystalline silicates in the subducting oceanic crust because the temperature of the slab is much lower than that of the normal mantle.<sup>69</sup> The noncrystalline basalts may convert to crystalline phases in contact with hydrothermal fluids. Therefore, although speculative, the observed structural changes of such amorphous materials may be useful for tracking the irreversible compression–decompression pathways of the subducting crust. Further studies of the structural transitions occurring in natural amorphous phases constrain the details of such irreversible phase changes. Finally, the permanently densified structure depends on the path taken to reach ambient pressure and room temperature because we studied the irreversible structural transitions occurring in a metastable phase. Because the structural transition at high pressure and the subsequent decompression are kinetically broadened, the kinetics of structural relaxation under decompression may be responsible for the remarkable resemblance between the residual density and the Al coordination change with a pronounced plateau (Figure 4). An additional kinetic study of structural relaxation after decompression remains. Whereas this study focuses on the structural transitions in short-range structures, the nature of the pressure-induced changes in medium-range structures that are responsible for the densification during extreme compression and subsequent decompression remains to be considered.

## ■ MATERIALS AND METHODS

**Sample Preparation.**  $\text{Mg}_3\text{Al}_2\text{Si}_3\text{O}_{12}$  (pyrope) glasses were synthesized from mixtures of  $\text{Al}_2\text{O}_3$ , MgO sintered at 1300 °C for 2 h, and 40%  $^{17}\text{O}$ -enriched  $\text{SiO}_2$ . We added ~0.2 wt % cobalt oxide to increase the S/N ratio of the NMR spectra by reducing the relaxation time of nuclear spins. The powder mixtures were melted at 1625 °C in an Ar environment for 1 h in a tube furnace. The melts formed in a Pt crucible were quenched into glasses. The composition of the glass is expected to be close to the nominal pyrope composition, as also inferred from a negligible weight loss (~1 wt %) during synthesis. (See ref 46 and references therein.) The glass sample was loaded and then sealed in a Pt capsule. The  $^{17}\text{O}$ -enriched pyrope glass was loaded in a scaled-up Kawai-type multianvil cell (Okayama University, Japan). A 14/6 (octahedron edge

length of the cell/truncated edge length of the anvils) assembly was used to compress the glass up to 24 GPa at room temperature for 1 h,<sup>70</sup> which was then decompressed with an approximate rate of 0.5 GPa/h. Whereas the decompression rate may affect the overall structures of recovered glasses, the time scale of structural transition is still expected to be much faster than the decompression rate. In addition, an 18/11 cell assembly was used to compress the glass to 6–15 GPa pressure at room temperature for 1 to 12 h,<sup>70,71</sup> which was then decompressed at the same rate. Structural relaxation may occur after decompression; however, the change may be very minor. The relaxation effect remains to be explored. The density of the glasses is not measured because the density measurement of compressed glass with a limited sample volume is currently challenging. Further efforts to independently constrain the bulk density of the glasses are necessary.

**NMR Spectroscopy.** The multinuclear NMR spectra of pyrope glasses were collected using a Varian solid-state NMR 400 spectrometer (9.4 T) at 104.23 MHz (<sup>27</sup>Al), 54.23 MHz (<sup>17</sup>O), and 79.4 MHz (<sup>29</sup>Si) with a 3.2 mm Varian double-resonance probe (Seoul National University, Korea). <sup>27</sup>Al MAS NMR spectra were collected with a recycle delay of 1 s, an *rf* pulse length of 0.3  $\mu$ s ( $\sim 30^\circ$  for solids), and a spinning speed of 18 kHz and referenced to a 0.1 M AlCl<sub>3</sub> solution. <sup>27</sup>Al 3QMAS NMR spectra were collected using a fast-amplitude modulation (FAM)-based shifted-echo pulse sequence (consisting of hard pulses (3.0  $\mu$ s and 0.7  $\mu$ s) and an echo delay of  $\sim 500$   $\mu$ s, followed by a soft pulse (15  $\mu$ s)). (See ref 72 and references therein.) <sup>29</sup>Si MAS NMR spectra were collected with a single  $30^\circ$  pulse of  $\sim 0.6$   $\mu$ s, a recycle delay of 30 s, and a sample spinning speed of 11 kHz. The spectra were referenced to external tetramethylsilane solution. <sup>17</sup>O 3QMAS NMR spectra were collected using a FAM-based shifted-echo pulse sequence with a recycle delay of 1 s and a spinning speed of 14 kHz and were referenced to tap water as the external reference.

## ■ ASSOCIATED CONTENT

### SI Supporting Information

The Supporting Information is available free of charge at <https://pubs.acs.org/doi/10.1021/acs.jpcllett.0c00709>.

S1. Topological origin of permanent densification in amorphous oxides at room temperature: earlier efforts. S2. Probing pressure-induced structural changes in aluminosilicate glasses at high pressure: insights from solid-state NMR. S3. Calibration of <sup>[n]</sup>Al fraction in <sup>27</sup>Al 3QMAS NMR spectra for the glasses. S4. Estimation of  $p_{0.5}$  and  $\alpha'$  of the oxide glasses. Table S1. Fitting parameters ( $p_{0.5}$  and  $\alpha$ ) for the <sup>[5,6]</sup>Al coordination number for pyrope glass and the residual densities for diverse oxide glasses. Figure S1. Changes in the normalized residual densities in oxide glasses (including alkali silicate, aluminosilicate, and borate glasses) with normalized pressure in diverse oxide glasses. Figure S2. Variation of normalized residual density with respect to varying pressure in oxide glasses. SI references (PDF)

## ■ AUTHOR INFORMATION

### Corresponding Author

**Sung Keun Lee** – Laboratory of Physics and Chemistry of Earth Materials, School of Earth and Environmental Sciences and Institute of Applied Physics, Seoul National University, Seoul

08826, Korea; [orcid.org/0000-0002-3149-3421](https://orcid.org/0000-0002-3149-3421);  
Email: [sungklee@snu.ac.kr](mailto:sungklee@snu.ac.kr)

### Authors

**Kwan Young Mun** – Laboratory of Physics and Chemistry of Earth Materials, School of Earth and Environmental Sciences, Seoul National University, Seoul 08826, Korea

**Yong-Hyun Kim** – Laboratory of Physics and Chemistry of Earth Materials, School of Earth and Environmental Sciences, Seoul National University, Seoul 08826, Korea

**Juho Lee** – Laboratory of Physics and Chemistry of Earth Materials, School of Earth and Environmental Sciences, Seoul National University, Seoul 08826, Korea

**Takuo Okuchi** – Institute for Planetary Materials, Okayama University, Misasa 682-0193, Japan; [orcid.org/0000-0001-6907-0945](https://orcid.org/0000-0001-6907-0945)

**Jung-Fu Lin** – Department of Geological Sciences, Jackson School of Geosciences, The University of Texas at Austin, Austin, Texas 78712, United States

Complete contact information is available at:  
<https://pubs.acs.org/10.1021/acs.jpcllett.0c00709>

### Notes

The authors declare no competing financial interest.

## ■ ACKNOWLEDGMENTS

This work was supported by the National Research Foundation, Korea (2017-053-046) to S.K.L. J.-F.L. acknowledges support from the National Science Foundation (NSF) of the United States (EAR-1916941) and the Visiting Scholar Program at the Institute for Planetary Materials, Okayama University at Misasa. T.O. acknowledges support from JSPS KAKENHI (17H01172). We are grateful for the constructive comments and suggestions by two anonymous reviewers, which greatly improved the quality and clarity of the manuscript.

## ■ REFERENCES

- (1) Elliot, S. R. *Physics of Amorphous Materials*; John Wiley & Sons, 1988.
- (2) Vandembroucq, D.; Deschamps, T.; Coussa, C.; Perriot, A.; Barthel, E.; Champagnon, B.; Martinet, C. Density Hardening Plasticity and Mechanical Ageing of Silica Glass under Pressure: A Raman Spectroscopic Study. *J. Phys.: Condens. Matter* **2008**, *20*, 485221.
- (3) Trachenko, K.; Dove, M. T.; Brazhkin, V.; El'kin, F. S. Network Rigidity and Properties of SiO<sub>2</sub> and GeO<sub>2</sub> Glasses under Pressure. *Phys. Rev. Lett.* **2004**, *93*, 135502.
- (4) Deschamps, T.; Margueritat, J.; Martinet, C.; Mermet, A.; Champagnon, B. Elastic Moduli of Permanently Densified Silica Glasses. *Sci. Rep.* **2015**, *4*, 7193.
- (5) Rouxel, T.; Ji, H.; Hammouda, T.; Moreac, A. Poisson's Ratio and the Densification of Glass under High Pressure. *Phys. Rev. Lett.* **2008**, *100*, 225501.
- (6) Januchta, K.; Stepniewska, M.; Jensen, L. R.; Zhang, Y.; Somers, M. A. J.; Bauchy, M.; Yue, Y.; Smedskjaer, M. M. Breaking the Limit of Micro-Ductility in Oxide Glasses. *Advanced Science* **2019**, *6*, 1901281.
- (7) Januchta, K.; Smedskjaer, M. M. Indentation Deformation in Oxide Glasses: Quantification, Structural Changes, and Relation to Cracking. *Journal of Non-Crystalline Solids: X* **2019**, *1*, 100007.
- (8) Ji, H.; Keryvin, V.; Rouxel, T.; Hammouda, T. Densification of Window Glass under Very High Pressure and Its Relevance to Vickers Indentation. *Scr. Mater.* **2006**, *55*, 1159–1162.

- (9) Kapoor, S.; Guo, X. J.; Youngman, R. E.; Hogue, C. L.; Mauro, J. C.; Rzoska, S. J.; Bockowski, M.; Jensen, L. R.; Smedskjaer, M. M. Network Glasses under Pressure: Permanent Densification in Modifier-Free  $\text{Al}_2\text{O}_3\text{-B}_2\text{O}_3\text{-P}_2\text{O}_5\text{-SiO}_2$  Systems. *Phys. Rev. Appl.* **2017**, *7*, 054011.
- (10) Molnar, G.; Ganster, P.; Tanguy, A. Effect of Composition and Pressure on the Shear Strength of Sodium Silicate Glasses: An Atomic Scale Simulation Study. *Phys. Rev. E: Stat. Phys., Plasmas, Fluids, Relat. Interdiscip. Top.* **2017**, *95*, 043001.
- (11) Devine, R. A. B.; Arndt, J. Si-O Bond-Length Modification in Pressure-Densified Amorphous  $\text{SiO}_2$ . *Phys. Rev. B: Condens. Matter Mater. Phys.* **1987**, *35*, 9376–9379.
- (12) Martinet, C.; Kassir-Bodon, A.; Deschamps, T.; Cornet, A.; Le Floch, S.; Martinez, V.; Champagnon, B. Permanently Densified  $\text{SiO}_2$  Glasses: A Structural Approach. *J. Phys.: Condens. Matter* **2015**, *27*, 325401.
- (13) Meade, C.; Hemley, R. J.; Mao, H. K. High-Pressure X-Ray Diffraction of  $\text{SiO}_2$  Glass. *Phys. Rev. Lett.* **1992**, *69*, 1387–1390.
- (14) Huang, L. P.; Kieffer, J. Amorphous-Amorphous Transitions in Silica Glass. II. Irreversible Transitions and Densification Limit. *Phys. Rev. B: Condens. Matter Mater. Phys.* **2004**, *69*, 224204.
- (15) Huang, L. P.; Kieffer, J. Amorphous-Amorphous Transitions in Silica Glass. I. Reversible Transitions and Thermomechanical Anomalies. *Phys. Rev. B: Condens. Matter Mater. Phys.* **2004**, *69*, 224203.
- (16) Sampath, S.; Benmore, C. J.; Lantzy, K. M.; Neufeind, J.; Leinenweber, K.; Price, D. L.; Yarger, J. L. Intermediate-Range Order in Permanently Densified  $\text{GeO}_2$  Glass. *Phys. Rev. Lett.* **2003**, *90*, 115502.
- (17) Guerette, M.; Poltorak, A.; Fei, Y.; Strobel, T. A. Permanent Densification of Silica Glass for Pressure Calibration between 9 and 20 GPa at Ambient Temperature. *High Pressure Res.* **2019**, *39*, 117–130.
- (18) Inamura, Y.; Katayama, Y.; Utsumi, W.; Funakoshi, K. Transformations in the Intermediate-Range Structure of  $\text{SiO}_2$  Glass under High Pressure and Temperature. *Phys. Rev. Lett.* **2004**, *93*, 015501.
- (19) Sato, T.; Funamori, N.; Yagi, T. Differential Strain and Residual Anisotropy in Silica Glass. *J. Appl. Phys.* **2013**, *114*, 103509.
- (20) Zha, C. S.; Hemley, R. J.; Mao, H. K.; Duffy, T. S.; Meade, C. Acoustic Velocities and Refractive-Index of  $\text{SiO}_2$  Glass to 57.5 GPa by Brillouin-Scattering. *Phys. Rev. B: Condens. Matter Mater. Phys.* **1994**, *50*, 13105–13112.
- (21) Sugai, S.; Onodera, A. Medium-Range Order in Permanently Densified  $\text{SiO}_2$  and  $\text{GeO}_2$  Glass. *Phys. Rev. Lett.* **1996**, *77*, 4210–4213.
- (22) Zanatta, M.; Baldi, G.; Brusa, R. S.; Egger, W.; Fontana, A.; Gilioli, E.; Mariuzzi, S.; Monaco, G.; Ravelli, L.; Sacchetti, F. Structural Evolution and Medium Range Order in Permanently Densified Vitreous  $\text{SiO}_2$ . *Phys. Rev. Lett.* **2014**, *112*, 045501.
- (23) Clark, A. N.; Leshner, C. E.; Jacobsen, S. D.; Sen, S. Mechanisms of Anomalous Compressibility of Vitreous Silica. *Phys. Rev. B: Condens. Matter Mater. Phys.* **2014**, *90*, 174110.
- (24) Drewitt, J. W. E.; Salmon, P. S.; Barnes, A. C.; Klotz, S.; Fischer, H. E.; Crichton, W. A. Structure of  $\text{GeO}_2$  Glass at Pressures up to 8.6 GPa. *Phys. Rev. B: Condens. Matter Mater. Phys.* **2010**, *81*, 014202.
- (25) Hemley, R. J.; Meade, C.; Mao, H. K. Medium-Range Order in Permanently Densified  $\text{SiO}_2$  and  $\text{GeO}_2$  Glass - Comment. *Phys. Rev. Lett.* **1997**, *79*, 1420–1420.
- (26) Liang, Y.; Miranda, C. R.; Scandolo, S. Temperature-Induced Densification of Compressed  $\text{SiO}_2$  Glass: A Molecular Dynamics Study. *High Pressure Res.* **2008**, *28*, 35–44.
- (27) Lee, S. K.; Eng, P. J.; Mao, H. K.; Meng, Y.; Newville, M.; Hu, M. Y.; Shu, J. F. Probing of Bonding Changes in  $\text{B}_2\text{O}_3$  Glasses at High Pressure with Inelastic X-Ray Scattering. *Nat. Mater.* **2005**, *4*, 851–854.
- (28) Huang, L.; Nicholas, J.; Kieffer, J.; Bass, J. Polyamorphic Transitions in Vitreous  $\text{B}_2\text{O}_3$  under Pressure. *J. Phys.: Condens. Matter* **2008**, *20*, 075107.
- (29) Liang, Y. F.; Miranda, C. R.; Scandolo, S. Mechanical Strength and Coordination Defects in Compressed Silica Glass: Molecular Dynamics Simulations. *Phys. Rev. B: Condens. Matter Mater. Phys.* **2007**, *75*, 024205.
- (30) Trease, N. M.; Clark, T. M.; Grandinetti, P. J.; Stebbins, J. F.; Sen, S. Bond Length-Bond Angle Correlation in Densified Silica-Results from O-17 NMR Spectroscopy. *J. Chem. Phys.* **2017**, *146*, 184505.
- (31) Williams, Q.; Jeanloz, R. Spectroscopic Evidence for Pressure-Induced Coordination Changes in Silicate-Glasses and Melts. *Science* **1988**, *239*, 902–905.
- (32) Lacks, D. J. Localized Mechanical Instabilities and Structural Transformations in Silica Glass under High Pressure. *Phys. Rev. Lett.* **1998**, *80*, 5385–5388.
- (33) Ryu, E.; Wakabayashi, D.; Koura, A.; Shimojo, F. Ab Initio Simulation of Permanent Densification in Silica Glass. *Phys. Rev. B: Condens. Matter Mater. Phys.* **2017**, *96*, 054206.
- (34) Tse, J. S.; Klug, D. D.; Lepage, Y. High-Pressure Densification of Amorphous Silica. *Phys. Rev. B: Condens. Matter Mater. Phys.* **1992**, *46*, 5933–5938.
- (35) Gleason, A. E.; Bolme, C. A.; Lee, H. J.; Nagler, B.; Galtier, E.; Kraus, R. G.; Sandberg, R.; Yang, W.; Langenhorst, F.; Mao, W. L. Time-Resolved Diffraction of Shock-Released  $\text{SiO}_2$  and Diaplectic Glass Formation. *Nat. Commun.* **2017**, *8*, 1481.
- (36) Guerette, M.; Ackerson, M. R.; Thomas, J.; Yuan, F. L.; Watson, E. B.; Walker, D.; Huang, L. P. Structure and Properties of Silica Glass Densified in Cold Compression and Hot Compression. *Sci. Rep.* **2015**, *5*, 15343.
- (37) Poe, B. T.; Romano, C.; Henderson, G. Raman and Xanes Spectroscopy of Permanently Densified Vitreous Silica. *J. Non-Cryst. Solids* **2004**, *341*, 162–169.
- (38) Rountree, C. L.; Vandembroucq, D.; Talamali, M.; Bouchaud, E.; Roux, S. Plasticity-Induced Structural Anisotropy of Silica Glass. *Phys. Rev. Lett.* **2009**, *102*, 195501.
- (39) Smedskjaer, M. M.; Youngman, R. E.; Striepe, S.; Potuzak, M.; Bauer, U.; Deubener, J.; Behrens, H.; Mauro, J. C.; Yue, Y. Irreversibility of Pressure Induced Boron Speciation Change in Glass. *Sci. Rep.* **2015**, *4*, 3770.
- (40) Kapoor, S.; Youngman, R. E.; Ma, L.; Lönnroth, N.; Rzoska, S. J.; Bockowski, M.; Jensen, L. R.; Bauchy, M.; Smedskjaer, M. M. Permanent Densification of Calcium Aluminophosphate Glasses. *Front. Mater.* **2019**, *6*, 63.
- (41) Januchta, K.; Youngman, R. E.; Goel, A.; Bauchy, M.; Logunov, S. L.; Rzoska, S. J.; Bockowski, M.; Jensen, L. R.; Smedskjaer, M. M. Discovery of Ultra-Crack-Resistant Oxide Glasses with Adaptive Networks. *Chem. Mater.* **2017**, *29*, 5865–5876.
- (42) Amin, S. A.; Leinenweber, K.; Benmore, C. J.; Weber, R.; Yarger, J. L. Characterizing Pressure-Induced Coordination Changes in  $\text{CaAl}_2\text{O}_4$  Glass Using Al-27 NMR. *J. Phys. Chem. C* **2012**, *116*, 2068–2073.
- (43) Shu, Y.; Kono, Y.; Ohira, I.; Li, Q.; Hrubik, R.; Park, C.; Kenney-Benson, C.; Wang, Y.; Shen, G. Observation of 9-Fold Coordinated Amorphous  $\text{Tio}_2$  at High Pressure. *J. Phys. Chem. Lett.* **2020**, *11*, 374–379.
- (44) Lee, S. K.; Kim, Y.-H.; Yi, Y. S.; Chow, P.; Xiao, Y.; Ji, C.; Shen, G. Oxygen Quadclusters in  $\text{SiO}_2$  Glass above Megabar Pressures up to 160 GPa Revealed by X-Ray Raman Scattering. *Phys. Rev. Lett.* **2019**, *123*, 235701.
- (45) Frankberg, E. J.; et al. Highly Ductile Amorphous Oxide at Room Temperature and High Strain Rate. *Science* **2019**, *366*, 864.
- (46) Lee, S. K.; Kim, H. I.; Kim, E. J.; Mun, K. Y.; Ryu, S. Extent of Disorder in Magnesium Aluminosilicate Glasses: Insights from Al-27 and O-17 NMR. *J. Phys. Chem. C* **2016**, *120*, 737–749.
- (47) Lee, S. K.; Kim, Y.-H.; Chow, P.; Xiao, Y.; Ji, C.; Shen, G. Amorphous Boron Oxide at Megabar Pressures Via Inelastic X-Ray Scattering. *Proc. Natl. Acad. Sci. U. S. A.* **2018**, *115*, 5855–5860.
- (48) Allwardt, J. R.; Stebbins, J. F.; Schmidt, B. C.; Frost, D. J.; Withers, A. C.; Hirschmann, M. M. Aluminum Coordination and the

Densification of High-Pressure Aluminosilicate Glasses. *Am. Mineral.* **2005**, *90*, 1218–1222.

(49) Lee, S. K. Structure of Silicate Glasses and Melts at High Pressure: Quantum Chemical Calculations and Solid-State Nmr. *J. Phys. Chem. B* **2004**, *108*, 5889–5900.

(50) Lee, S. K. Simplicity in Melt Densification in Multicomponent Magmatic Reservoirs in Earth's Interior Revealed by Multinuclear Magnetic Resonance. *Proc. Natl. Acad. Sci. U. S. A.* **2011**, *108*, 6847–6852.

(51) Xue, X.; Stebbins, J. F.; Kanzaki, M. Correlations between O-17 NMR Parameters and Local Structure around Oxygen in High-Pressure Silicates and the Structure of Silicate Melts at High Pressure. *Am. Mineral.* **1994**, *79*, 31–42.

(52) Yarger, J. L.; Smith, K. H.; Nieman, R. A.; Diefenbacher, J.; Wolf, G. H.; Poe, B. T.; McMillan, P. F. Al Coordination Changes in High-Pressure Aluminosilicate Liquids. *Science* **1995**, *270*, 1964–1967.

(53) Lee, S. K. Effect of Pressure on Structure of Oxide Glasses at High Pressure: Insights from Solid-State Nmr of Quadrupolar Nuclei. *Solid State Nucl. Magn. Reson.* **2010**, *38*, 45–57.

(54) Lee, S. K.; Cody, G. D.; Fei, Y. W.; Mysen, B. O. Nature of Polymerization and Properties of Silicate Melts and Glasses at High Pressure. *Geochim. Cosmochim. Acta* **2004**, *68*, 4189–4200.

(55) Ohira, I.; Kono, Y.; Shibazaki, Y.; Kenney-Benson, C.; Masuno, A.; Shen, G. Ultrahigh Pressure Structural Changes in a 60 Mol.% Al<sub>2</sub>O<sub>3</sub>-40 Mol.% SiO<sub>2</sub> Glass. *Geochem. Perspect. Lett.* **2019**, *10*, 41–45.

(56) Lee, S. K.; Eng, P. J.; Mao, H. K.; Shu, J. F. Probing and Modeling of Pressure-Induced Coordination Transformation in Borate Glasses: Inelastic X-Ray Scattering Study at High Pressure. *Phys. Rev. B: Condens. Matter Mater. Phys.* **2008**, *78*, 214203.

(57) Lee, S. K.; Yi, Y. S.; Cody, G. D.; Mibe, K.; Fei, Y. W.; Mysen, B. O. Effect of Network Polymerization on the Pressure-Induced Structural Changes in Sodium Aluminosilicate Glasses and Melts: Al-27 and O-17 Solid-State Nmr Study. *J. Phys. Chem. C* **2012**, *116*, 2183–2191.

(58) Wakabayashi, D.; Funamori, N.; Sato, T.; Taniguchi, T. Compression Behavior of Densified SiO<sub>2</sub> Glass. *Phys. Rev. B: Condens. Matter Mater. Phys.* **2011**, *84*, 144103.

(59) Keryvin, V.; Meng, J. X.; Gicquel, S.; Guin, J. P.; Charleux, L.; Sangleboeuf, J. C.; Pilvin, P.; Rouxel, T.; Le Quilliec, G. Constitutive Modeling of the Densification Process in Silica Glass under Hydrostatic Compression. *Acta Mater.* **2014**, *62*, 250–257.

(60) Bridgman, P. W.; Simon, I. Effects of Very High Pressures on Glass. *J. Appl. Phys.* **1953**, *24*, 405–413.

(61) Della Valle, R. G.; Venuti, E. High-Pressure Densification of Silica Glass: A Molecular-Dynamics Simulation. *Phys. Rev. B: Condens. Matter Mater. Phys.* **1996**, *54*, 3809–3816.

(62) Rouxel, T.; Ji, H.; Guin, J. P.; Augereau, F.; Rufflé, B. Indentation Deformation Mechanism in Glass: Densification Versus Shear Flow. *J. Appl. Phys.* **2010**, *107*, 094903.

(63) Deschamps, T.; Kassir-Bodon, A.; Sonnevile, C.; Margueritat, J.; Martinet, C.; de Ligny, D.; Mermet, A.; Champagnon, B. Permanent Densification of Compressed Silica Glass: A Raman-Density Calibration Curve. *J. Phys.: Condens. Matter* **2013**, *25*, 025402.

(64) Wu, J. S.; Gross, T. M.; Huang, L. P.; Jaccani, S. P.; Youngman, R. E.; Rzoska, S. J.; Bockowski, M.; Bista, S.; Stebbins, J. F.; Smedskjaer, M. M. Composition and Pressure Effects on the Structure, Elastic Properties and Hardness of Aluminoborosilicate Glass. *J. Non-Cryst. Solids* **2020**, *530*, 119797.

(65) Zeidler, A.; Salmon, P. S.; Skinner, L. B. Packing and the Structural Transformations in Liquid and Amorphous Oxides from Ambient to Extreme Conditions. *Proc. Natl. Acad. Sci. U. S. A.* **2014**, *111*, 10045–10048.

(66) Kim, Y.-H.; Yi, Y. S.; Kim, H.-I.; Chow, P.; Xiao, Y.; Shen, G.; Lee, S. K. Structural Transitions in MgSiO<sub>3</sub> Glasses and Melts at the Core-Mantle Boundary Observed Via Inelastic X-Ray Scattering. *Geophys. Res. Lett.* **2019**, *46*, 13756–13764.

(67) Wu, J. S.; Deubener, J.; Stebbins, J. F.; Grygarova, L.; Behrens, H.; Wondraczek, L.; Yue, Y. Z. Structural Response of a Highly Viscous Aluminoborosilicate Melt to Isotropic and Anisotropic Compressions. *J. Chem. Phys.* **2009**, *131*, 104504.

(68) Tsiok, O. B.; Brazhkin, V. V.; Lyapin, A. G.; Khvostantsev, L. G. Logarithmic Kinetics of the Amorphous-Amorphous Transformations in SiO<sub>2</sub> and GeO<sub>2</sub> Glasses under High-Pressure. *Phys. Rev. Lett.* **1998**, *80*, 999–1002.

(69) Xu, C.; Kynicky, J.; Song, W.; Tao, R.; Lu, Z.; Li, Y.; Yang, Y.; Pohanka, M.; Galiova, M. V.; Zhang, L.; et al. Cold Deep Subduction Recorded by Remnants of a Paleoproterozoic Carbonated Slab. *Nat. Commun.* **2018**, *9*, 2790.

(70) Okuchi, T.; Purevjav, N.; Tomioka, N.; Lin, J.-F.; Kuribayashi, T.; Schoneveld, L.; Hwang, H.; Sakamoto, N.; Kawasaki, N.; Yurimoto, H. Synthesis of Large and Homogeneous Single Crystals of Water-Bearing Minerals by Slow Cooling at Deep-Mantle Pressures. *Am. Mineral.* **2015**, *100*, 1483–1492.

(71) Frost, D. J.; Poe, B. T.; Trønnes, R. G.; Liebske, C.; Duba, A.; Rubie, D. C. A New Large-Volume Multianvil System. *Phys. Earth Planet. Inter.* **2004**, *143–144*, 507–514.

(72) Lee, S. K.; Ryu, S. Probing of Triply Coordinated Oxygen in Amorphous Al<sub>2</sub>O<sub>3</sub>. *J. Phys. Chem. Lett.* **2018**, *9*, 150–156.

(73) Ghosh, D. B.; Karki, B. B. First-Principles Molecular Dynamics Simulations of Anorthite (CaAl<sub>2</sub>Si<sub>2</sub>O<sub>8</sub>) Glass at High Pressure. *Phys. Chem. Miner.* **2018**, *45*, 575–587.